




## Research Article



# Temperature-dependent device properties of $\gamma$ -CuI and $\beta$ -Ga<sub>2</sub>O<sub>3</sub> heterojunctions

Rama Venkata Krishna Rao<sup>1</sup> · Ajinkya K. Ranade<sup>2</sup> · Pradeep Desai<sup>2</sup> · Golap Kalita<sup>2,3</sup> · Hiroo Suzuki<sup>1</sup> · Yasuhiko Hayashi<sup>1</sup> 

Received: 3 April 2021 / Accepted: 23 August 2021

Published online: 08 September 2021

© The Author(s) 2021 [OPEN](#)

## Abstract

Temperature-dependent studies of Ga<sub>2</sub>O<sub>3</sub>-based heterojunction devices are important in understanding its carrier transport mechanism, junction barrier potential, and stability at higher temperatures. In this study, we investigated the temperature-dependent device characteristics of the p-type  $\gamma$ -copper iodide ( $\gamma$ -CuI)/n-type  $\beta$ -gallium oxide ( $\beta$ -Ga<sub>2</sub>O<sub>3</sub>) heterojunctions, thereby revealing their interface properties. The fabricated  $\gamma$ -CuI/ $\beta$ -Ga<sub>2</sub>O<sub>3</sub> heterojunction showed excellent diode characteristics with a high rectification ratio and low reverse saturation current at 298 K in the presence of a large barrier height (0.632 eV). The temperature-dependent device characteristics were studied in the temperature range 273–473 K to investigate the heterojunction interface. With an increase in temperature, a gradual decrease in the ideality factor and an increase in the barrier height were observed, indicating barrier inhomogeneity at the heterojunction interface. Furthermore, the current–voltage measurement showed electrical hysteresis for the reverse saturation current, although it was not observed for the forward bias current. The presence of electrical hysteresis for the reverse saturation current and of the barrier inhomogeneity in the temperature-dependent characteristics indicates the presence of some level of interface states for the  $\gamma$ -CuI/ $\beta$ -Ga<sub>2</sub>O<sub>3</sub> heterojunction device. Thus, our study showed that the electrical hysteresis can be correlated with temperature-dependent electrical characteristics of the  $\beta$ -Ga<sub>2</sub>O<sub>3</sub>-based heterojunction device, which signifies the presence of surface defects and interface states.

## Article Highlights

- We revealed the interface properties of p-type  $\gamma$ -copper iodide ( $\gamma$ -CuI) and n-type  $\beta$ -gallium oxide ( $\beta$ -Ga<sub>2</sub>O<sub>3</sub>) heterojunction.
- The developed heterostructure showed a large barrier height (0.632 eV) at the interface, which is stable at a temperature as high as 473 K.
- We confirmed the current transport mechanism at the interface of the heterojunction by analyzing the temperature dependent current–voltage characterization.

✉ Yasuhiko Hayashi, hayashi.yasuhiko@okayama-u.ac.jp | <sup>1</sup>Graduate School of Natural Science and Technology, Okayama University, 3-1-1 Tsushima-naka, Kita, Okayama 700-8530, Japan. <sup>2</sup>Department of Physical Science and Engineering, Nagoya Institute of Technology, Gokiso-Cho, Showa-ku, Nagoya 466-8555, Japan. <sup>3</sup>Frontier Research Institute for Material Science, Nagoya Institute of Technology, Nagoya, Japan.



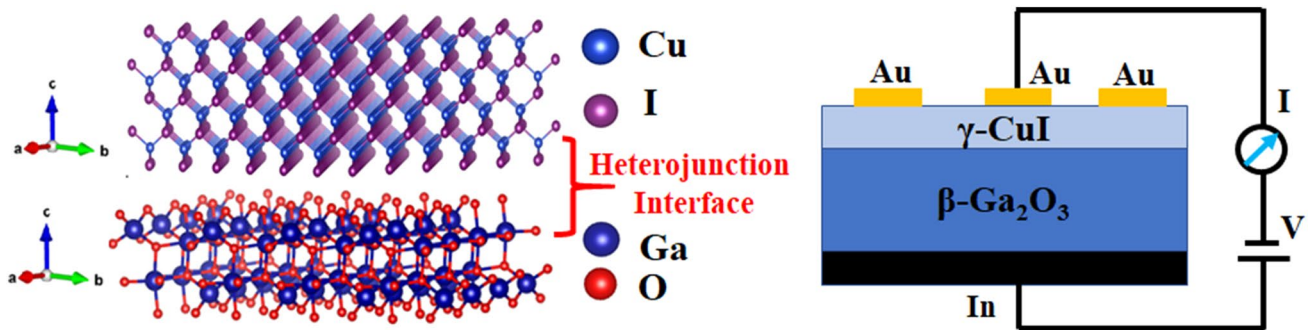
SN Applied Sciences

(2021) 3:796

| <https://doi.org/10.1007/s42452-021-04774-3>

SN Applied Sciences  
A **SPRINGER NATURE** journal

## Graphic abstract



**Keywords** Gallium oxide ·  $\gamma$ -copper iodide · Heterojunction · Device · Temperature dependent

## 1 Introduction

Among ultra-wide bandgap semiconductors, gallium oxide ( $\text{Ga}_2\text{O}_3$ ), with a bandgap of 4.5–4.9 eV, has attracted significant attention for deep ultraviolet (DUV) photonics and power electronic device applications [1, 2].  $\beta$ - $\text{Ga}_2\text{O}_3$ , with a monoclinic structure and lattice parameters of  $a = 12.22 \text{ \AA}$ ,  $b = 3.0 \text{ \AA}$ , and  $c = 5.8 \text{ \AA}$ , is the most stable form among all the polymorphs of  $\text{Ga}_2\text{O}_3$  at room temperature [3, 4]. It has been reported that electron mobility as high as  $300 \text{ cm}^2 \text{ V}^{-1} \text{ s}^{-1}$  can be achieved in  $\beta$ - $\text{Ga}_2\text{O}_3$  at room temperature.  $\beta$ - $\text{Ga}_2\text{O}_3$  possesses a critical field strength higher than that of Si, SiC, and GaN semiconducting materials. The predicted critical field ( $E_{br}$ ) for  $\beta$ - $\text{Ga}_2\text{O}_3$  is  $8 \text{ MV cm}^{-1}$ , whereas the measured  $E_{br}$  is  $3.8 \text{ MV cm}^{-1}$  [5]. Owing to its high chemical and mechanical stabilities (Young's modulus of  $\beta$ - $\text{Ga}_2\text{O}_3 = 232 \text{ GPa}$ ) and thermal stability (melting point  $1820 \text{ }^\circ\text{C}$ ), it is well suited for applications such as solar-blind photodetectors [6], light-emitting devices, and power electronic devices [7, 8].  $\beta$ - $\text{Ga}_2\text{O}_3$  exhibits n-type semiconducting behavior due to the presence of oxygen vacancies, similar to many other oxide semiconductors [9]. Most device fabrication approaches have adopted the Schottky junction or p-n heterojunction structure for practical applications [10, 11]. Thus, suitable materials for fabricating a Schottky or p-n junction of  $\text{Ga}_2\text{O}_3$  are critical in achieving high device performance.

$\beta$ - $\text{Ga}_2\text{O}_3$ -based Schottky barrier diodes (SBDs) have been investigated for the development of high-voltage devices as well as solar-blind photodetectors [10, 12, 13]. Metal electrodes, such as Au (gold), Pt (platinum), and Ni (nickel), have been explored for the fabrication of  $\beta$ - $\text{Ga}_2\text{O}_3$ -based SBDs [3, 4, 14, 15]. We have demonstrated the integration of graphene with  $\beta$ - $\text{Ga}_2\text{O}_3$  for the fabrication of deep-UV photo responsive SBD devices. SBDs are majority carrier devices, where the interface between the  $\text{Ga}_2\text{O}_3$  and metal contacts plays a significant role in the device

properties [14, 15]. By contrast, p-n junctions are minority carrier devices, which are important in achieving a low reverse saturation current and high breakdown voltage. Thus, a suitable p-type wide-bandgap semiconductor as a counterpart for the n-type  $\text{Ga}_2\text{O}_3$  is significant for device fabrication [15, 16].  $\gamma$ -CuI with a bandgap of  $\sim 3.1 \text{ eV}$  and p-type carrier mobility of  $\sim 40 \text{ cm}^2 \text{ V}^{-1} \text{ s}^{-1}$  has been investigated for heterojunction devices with  $\beta$ - $\text{Ga}_2\text{O}_3$  [17, 18]. The lattice mismatch between the cubic phase  $\gamma$ -CuI (111) and  $\beta$ - $\text{Ga}_2\text{O}_3$  along the c-axis is approximately 2%, indicating the possibility of fabricating a compatible heterostructure of  $\gamma$ -CuI (111) and  $\beta$ - $\text{Ga}_2\text{O}_3$  for heterojunction device applications [19–22].

Previously, Ranade et al. reported the integration of  $\gamma$ -CuI with gallium nitride (GaN), which is a III nitride wide-bandgap semiconductor, to form a p-n heterojunction with high-temperature stable photovoltaic action [18]. The successful fabrication of a  $\gamma$ -CuI/GaN heterojunction motivated us to explore the integration of p-type  $\gamma$ -CuI with  $\beta$ - $\text{Ga}_2\text{O}_3$ . In our previous study, we reported the observation of a DUV radiation-induced photovoltaic action for the  $\gamma$ -CuI/ $\beta$ - $\text{Ga}_2\text{O}_3$  heterojunction. In contrast to our previous studies, herein, we revealed the behavior of the heterojunction interface in the  $\gamma$ -CuI/ $\beta$ - $\text{Ga}_2\text{O}_3$  material system, which is significant for understanding its defect states, current transport mechanism, and temperature stability [23]. The temperature-dependent device characteristics were studied in the temperature range 273–473 K to investigate the heterojunction interface. With an increase in temperature, a gradual decrease in the ideality factor and an increase in barrier height were observed, indicating a barrier inhomogeneity at the heterojunction interface. Interestingly, we can correlate the electrical hysteresis and barrier inhomogeneity behavior of the  $\gamma$ -CuI/ $\beta$ - $\text{Ga}_2\text{O}_3$  heterojunction device, thereby revealing the influence of the interface states on these parameters.

## 2 Materials and methods

Here, we used Sn-doped, n-type single-crystal  $\beta$ - $\text{Ga}_2\text{O}_3$  (thickness of 650  $\mu\text{m}$ , donor concentration of  $3 \times 10^{18} \text{ cm}^{-3}$ ) purchased from Tamura Corporation, Japan. Approximately 0.05 g of copper iodide ( $\gamma$ -Cul) powder (purity  $\sim 95\%$ ), purchased from Wako Pure Chemical Industries Ltd., was evaporated for 2 min in a vacuum chamber at a pressure of  $\sim 10^{-3}$  Pa and an applied current of 35 mA. The thickness of the  $\gamma$ -Cul layer was controlled by varying the deposition duration. Metal electrodes were deposited on the fabricated  $\gamma$ -Cul/ $\beta$ - $\text{Ga}_2\text{O}_3$  heterostructure to complete the device structure. Gold (Au) and indium (In) electrodes were deposited on top of the  $\gamma$ -Cul and backside of the  $\beta$ - $\text{Ga}_2\text{O}_3$ , respectively, using a metal shadow mask with a thermal evaporator instrument under a high vacuum ( $\sim 10^{-3}$  Pa). The Cul/ $\beta$ - $\text{Ga}_2\text{O}_3$  heterostructure samples were characterized using X-ray diffraction (XRD), UV–Vis absorption spectroscopy, and Raman spectroscopy. XRD studies were carried out using a Rigaku Smart Lab SE with Cu K $\alpha$  radiation as the X-ray source ( $\lambda_{\text{av}} = 1.5406 \text{ \AA}$ ). The surface of the heterostructure was analyzed using a JEOL JSM 5600 scanning electron microscope (SEM) at an accelerating voltage of 20 kV. Raman spectroscopy measurements on the  $\beta$ - $\text{Ga}_2\text{O}_3$  and deposited Cul film were performed using an NRS 3300 laser Raman spectrometer at a laser excitation wavelength of 532.08 nm. UV–Vis absorption spectroscopy analysis was performed using a JASCO V-670 K spectrophotometer. The Cul film and Au and In metal electrodes were deposited using a ULVAC VPC-260F thermal evaporator. Current density–voltage (J–V) measurements were carried out using a two-probe system and a Keithley 2401 source meter at different device temperatures. The J–V characteristics of the heterostructure were analyzed at different temperatures (298–473 K) on a hot plate using a digital temperature controller.

## 3 Results and discussion

Figure 1a shows the XRD spectra of the  $\beta$ - $\text{Ga}_2\text{O}_3$  substrate and the fabricated  $\gamma$ -Cul/ $\beta$ - $\text{Ga}_2\text{O}_3$  heterostructure. A strong diffraction peak at  $61.01^\circ$  corresponding to the (020) reflection phase of  $\beta$ - $\text{Ga}_2\text{O}_3$  was observed in both samples. Again, an additional high-intensity peak is observed at  $26.06^\circ$  corresponding to the (111) plane of the cubic-phase  $\gamma$ -Cul for the  $\gamma$ -Cul/ $\beta$ - $\text{Ga}_2\text{O}_3$  heterostructure sample, which is in accordance with the JCPDS Card number 06-0246 [24, 25]. The predominantly (111)-oriented cubic-phase  $\gamma$ -Cul was obtained on the monoclinic  $\beta$ - $\text{Ga}_2\text{O}_3$  single-crystal substrate, which is consistent with previously reported results [21, 22]. Figure 1b shows the

Raman scattering spectra of the single-crystal  $\beta$ - $\text{Ga}_2\text{O}_3$  substrate and the  $\gamma$ -Cul/ $\beta$ - $\text{Ga}_2\text{O}_3$  heterostructure. The low-frequency Raman peaks at 146, 17, and 201  $\text{cm}^{-1}$  denote the liberation and translation of the tetrahedral/octahedral chains. The mid-frequency Raman peaks at 348, 417, and 476  $\text{cm}^{-1}$  are related to the distortion of the  $\text{Ga}_2\text{O}_6$  octahedra. The high-frequency Raman peaks at 631, 654, and 767  $\text{cm}^{-1}$  indicate the stretching and bending of the  $\text{GaO}_4$  tetrahedra, as shown in Fig. 1b. The high-intensity  $A_g$  Raman mode at 200  $\text{cm}^{-1}$  signifies the high-quality crystalline nature of the  $\beta$ - $\text{Ga}_2\text{O}_3$  sample used for the device fabrication [20]. Further, by analyzing the Raman spectra of the fabricated heterostructure, we observed an additional peak at 119  $\text{cm}^{-1}$ , corresponding to the deposited  $\gamma$ -Cul film on the  $\beta$ - $\text{Ga}_2\text{O}_3$  substrate. The XRD spectra of the  $\beta$ - $\text{Ga}_2\text{O}_3$  substrate and the  $\gamma$ -Cul/ $\beta$ - $\text{Ga}_2\text{O}_3$  sample can be correlated with the Raman analysis of the purity and crystalline nature of the prepared samples for the device fabrication. Figure 1c shows the UV absorption spectra of the  $\gamma$ -Cul film deposited on a glass substrate in comparison to the absorption spectra of  $\beta$ - $\text{Ga}_2\text{O}_3$ . The  $\gamma$ -Cul film shows absorption peaks in the range of 350–400 nm, whereas the absorption for the  $\beta$ - $\text{Ga}_2\text{O}_3$  sample was obtained in the range of 190–280 nm. Thus, the bandgap width for the  $\gamma$ -Cul/ $\beta$ - $\text{Ga}_2\text{O}_3$  heterojunction was 190–400 nm. Figure 1d shows the Tauc plot for calculating the optical bandgap of the deposited  $\gamma$ -Cul film, which was computed as 3.02 eV, consistent with previously reported values [26]. A Tauc plot of the  $\beta$ - $\text{Ga}_2\text{O}_3$  sample was plotted for comparison with the Tauc plot of the  $\gamma$ -Cul film. The optical band gap of  $\beta$ - $\text{Ga}_2\text{O}_3$  was computed as 4.6 eV, which agrees with the theoretical value [1, 27]. Furthermore, the optical absorption study and the obtained bandgap can be correlated with the highly crystalline  $\beta$ - $\text{Ga}_2\text{O}_3$  and  $\gamma$ -Cul/ $\beta$ - $\text{Ga}_2\text{O}_3$  heterostructure samples, as observed from the Raman and XRD analyses. Figure 1e shows the SEM image of the thermally evaporated  $\gamma$ -Cul film on  $\beta$ - $\text{Ga}_2\text{O}_3$ . The thermally evaporated  $\gamma$ -Cul film on  $\beta$ - $\text{Ga}_2\text{O}_3$  showed a granular morphology, where the grain size of the  $\gamma$ -Cul and surface roughness may change with the deposition conditions. Figure 1f shows a tilted SEM image of the  $\gamma$ -Cul film on  $\beta$ - $\text{Ga}_2\text{O}_3$ , presenting the thickness of  $\gamma$ -Cul around 1  $\mu\text{m}$ . The thickness and uniformity of the film on the  $\beta$ - $\text{Ga}_2\text{O}_3$  substrate were controlled by the evaporation rate, where the thickness and uniformity of the  $\gamma$ -Cul film can significantly differ with the deposition rate. A heterojunction device was fabricated with the as-deposited  $\gamma$ -Cul film, where a persistent diode characteristic was obtained, as discussed next, with a device structure of Au/ $\gamma$ -Cul/ $\beta$ - $\text{Ga}_2\text{O}_3$ /In.

Figure 2a shows the cross-section stick and ball crystal structure of the  $\gamma$ -Cul and  $\beta$ - $\text{Ga}_2\text{O}_3$  device interface. The electron affinities of the n-type  $\beta$ - $\text{Ga}_2\text{O}_3$  and p-type  $\gamma$ -Cul were in the range of 4.0 and 2.1–2.2 eV, respectively, which

indicates the possibility of creating a large built-in field at the interface. The bandgaps of the two materials as calculated from the absorption spectra were 3.02 and 4.6 eV for  $\gamma$ -CuI and  $\beta$ -Ga<sub>2</sub>O<sub>3</sub>, respectively. As discussed here, owing to the large differences in the electron affinity and work function, a significant built-in field ( $\varphi_{\beta\text{-Ga}_2\text{O}_3} - \varphi_{\gamma\text{-CuI}} = V_{\text{bi}}$ ) can be obtained at the interface of the  $\gamma$ -CuI/ $\beta$ -Ga<sub>2</sub>O<sub>3</sub> heterojunction [18, 28]. Figure 2b shows a schematic diagram of the fabricated  $\gamma$ -CuI/ $\beta$ -Ga<sub>2</sub>O<sub>3</sub> vertical heterojunction device. The Au and In electrodes were deposited on  $\gamma$ -CuI and  $\beta$ -Ga<sub>2</sub>O<sub>3</sub>, respectively, to fabricate them. The Au electrode was deposited on  $\gamma$ -CuI considering the similar work function in the range of 5.1 eV. A work function in the range 4.08–4.12 eV was selected considering the electron affinity of n-type  $\beta$ -Ga<sub>2</sub>O<sub>3</sub> to be approximately 4.0 eV [23, 29]. The fabricated Au/ $\gamma$ -CuI/ $\beta$ -Ga<sub>2</sub>O<sub>3</sub>/In vertical heterojunction device was analyzed for its J–V characteristics. First, the device was analyzed at room temperature (298 K). Figure 2c shows the J–V characteristics at 298 K in the voltage range of –2 to +2 V under dark conditions. Good rectifying diode behavior was observed with low series resistance and a high rectification ratio ( $\sim 10^4$ ). Figure 2d shows the log plot of the J–V curve at room temperature. The diode characteristics can be compared with the previously reported results for  $\gamma$ -CuI/ $\beta$ -Ga<sub>2</sub>O<sub>3</sub> and diamond/ $\beta$ -Ga<sub>2</sub>O<sub>3</sub> heterojunction diodes [11, 20]. The diode ideality factor ( $n$ ), computed from the log plot, was found to be 3.5. The diode J–V characteristics can be expressed as follows, correlating the current and voltage with the ideality factor.

$$J = J_0 \left( e^{\frac{qV}{nkT}} - 1 \right), \quad (1)$$

where  $J$  is the current density flowing through the diode,  $V$  is the voltage across the diode,  $J_0$  is the saturation current density,  $T$  is the temperature in Kelvin,  $q$  is the electron charge, and  $k$  is the Boltzmann's constant. The  $n$  value determines the deviation from the ideal diode owing to the presence of a tunneling component and barrier inhomogeneity [30]. The ideality factor was higher than some of the previously reported values for  $\beta$ -Ga<sub>2</sub>O<sub>3</sub> heterojunction devices [11, 15, 21, 22, 31–34]. In addition, the reverse saturation current was significantly low in the fabricated device, as can be observed from the J–V characteristics. Thus, the deposited  $\gamma$ -CuI on  $\beta$ -Ga<sub>2</sub>O<sub>3</sub> is suitable for the fabrication of the vertical heterojunction device. Subsequently, we analyzed the temperature-dependent J–V characteristics to understand the current transport behavior at the heterojunction interface.

Figure 3a shows the temperature-dependent J–V characteristics of the Au/ $\gamma$ -CuI/ $\beta$ -Ga<sub>2</sub>O<sub>3</sub>/In heterojunction under an applied bias voltage of –2 to +2 V in the temperature range 298–373 K. The temperature-dependent analysis of the  $\gamma$ -CuI/ $\beta$ -Ga<sub>2</sub>O<sub>3</sub> heterostructure elucidated

the interface properties and compatibility of the material system for device fabrication. The fabricated device showed consistent rectification diode characteristics as the temperature was increased to 373 K. Figure 3b shows the log plot with an increasing temperature. The forward current consistently increased with increase in temperature (Fig. 3a); however, the change in current was not significantly high, because the variation in the logarithm plot was not noticeably visible. The saturation current is significantly low, because of which a small change in current is pronounced in the logarithm plot in the reverse bias voltage. The reverse saturation current was slightly non-saturated at the reverse bias voltage for the measured temperature range. This can be attributed to the barrier inhomogeneity at the interface of  $\gamma$ -CuI/ $\beta$ -Ga<sub>2</sub>O<sub>3</sub>. Subsequently, the barrier height ( $\varphi_{\text{B}}$ ) was analyzed by changing the temperature for the J–V characteristic using the reverse saturation current density equation.

$$J_0 = AA^* T^2 \text{Exp}\left(\frac{-q\varphi_{\text{B}}}{kT}\right), \quad (2)$$

where  $A^*$  is Richardson's constant ( $41 \text{ A cm}^{-2} \text{ K}^{-2}$  for  $\beta$ -Ga<sub>2</sub>O<sub>3</sub>),  $A$  is the contact area,  $q$  is the electron charge,  $T$  is the temperature in Kelvin,  $k$  is the Boltzmann constant, and  $\varphi_{\text{B}}$  is the effective barrier height.

Figure 3c shows the trends in  $n$  and  $\varphi_{\text{B}}$  at various temperatures.  $n$  decreased, and  $\varphi_{\text{B}}$  increased as the temperature increased from 298 to 373 K. The  $\varphi_{\text{B}}$  at the interface between  $\gamma$ -CuI and  $\beta$ -Ga<sub>2</sub>O<sub>3</sub> was approximately 0.632 eV at room temperature (298 K) from the J–V characteristics, which is relatively higher than those of other  $\beta$ -Ga<sub>2</sub>O<sub>3</sub> heterojunction devices. However, the measured barrier height was smaller than the theoretical value, as mentioned earlier, which may be due to the presence of a tunneling component at the heterojunction interface in the presence of the interface states [24].

Furthermore, the interface quality of the Au/ $\gamma$ -CuI/ $\beta$ -Ga<sub>2</sub>O<sub>3</sub>/In heterojunction was investigated. The J–V characteristics of the forward and reverse sweeps were measured to analyze the occurrence of electrical hysteresis under dark conditions. Figure 4a shows the forward and reverse sweeps under a bias voltage of +2 V. The measured J–V curve showed no hysteresis effect for the forward bias voltage. Figure 4b shows the logarithmic plot of the J–V characteristics with a small electrical hysteresis in the reverse saturation current. As the reverse saturation current is much smaller, the electrical hysteresis becomes more prominent. The presence of electrical hysteresis in the reverse saturation current indicates some level of interface states for the fabricated  $\gamma$ -CuI/ $\beta$ -Ga<sub>2</sub>O<sub>3</sub> heterojunction [29, 30]. Figure 4c shows the J–V characteristics of the fabricated device at 473 K, which still showed excellent rectification diode characteristics at a rectification ratio of

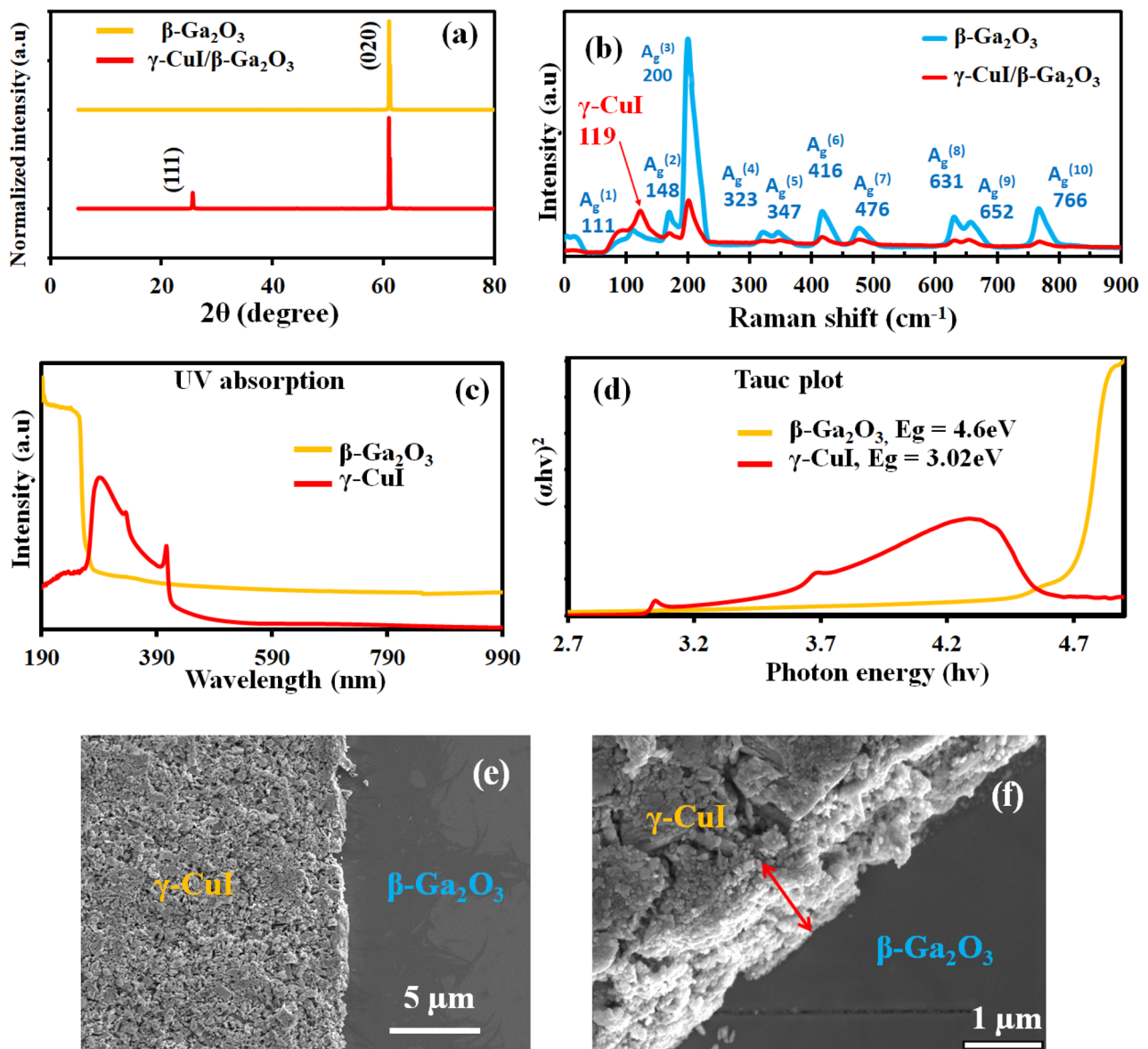


**Fig. 1** **a** X-ray diffraction pattern of the  $\beta\text{-Ga}_2\text{O}_3$  substrate and  $\gamma\text{-CuI}/\beta\text{-Ga}_2\text{O}_3$  heterostructure, **b** Raman spectra of the  $\beta\text{-Ga}_2\text{O}_3$  substrate and  $\gamma\text{-CuI}$  film, **c** UV absorption of the  $\beta\text{-Ga}_2\text{O}_3$  substrate and  $\gamma\text{-CuI}$  film, **d** Tauc plots, presenting the respective bandgap

of the two materials; SEM image of the  $\gamma\text{-CuI}$  film, **e** on top of the  $\beta\text{-Ga}_2\text{O}_3$  substrate and **f** a tilted view at the edge of the  $\gamma\text{-CuI}$  film on  $\beta\text{-Ga}_2\text{O}_3$

$10^2$ . Further, the J–V characteristic was also measured at 523 K; however, the device properties were not consistent, as a dark color appeared around the Au electrode due to oxidation. The study of the high-temperature stability of the  $\gamma\text{-CuI}/\beta\text{-Ga}_2\text{O}_3$  device is an important aspect to confirm the suitability of the fabricated heterojunction device. Figure 4d shows the probable energy band diagram for the  $\gamma\text{-CuI}/\beta\text{-Ga}_2\text{O}_3$  heterojunction device at equilibrium. The energy band diagram was configured from the electron affinity and bandgap values of n-type  $\beta\text{-Ga}_2\text{O}_3$  ( $\chi = 4.0$  eV;  $E_g = 3.02$  eV) and p-type  $\gamma\text{-CuI}$  ( $\chi = 2.1\text{--}2.2$  eV;  $E_g = 4.6$  eV).

Because the electron affinities of the two semiconductors are significantly different, a large band bending as well as a large barrier potential at the heterojunction interface can be estimated [24, 35–37]. The band diagram also represents the suitability of both the semiconductors for heterojunction device applications, where the formation of an interface with the deposition process can significantly affect the device performance. From the temperature-dependent analysis, it can be observed that the  $\gamma\text{-CuI}/\beta\text{-Ga}_2\text{O}_3$  heterojunction is quite stable with consistent highly rectifying diode characteristics. Most importantly,

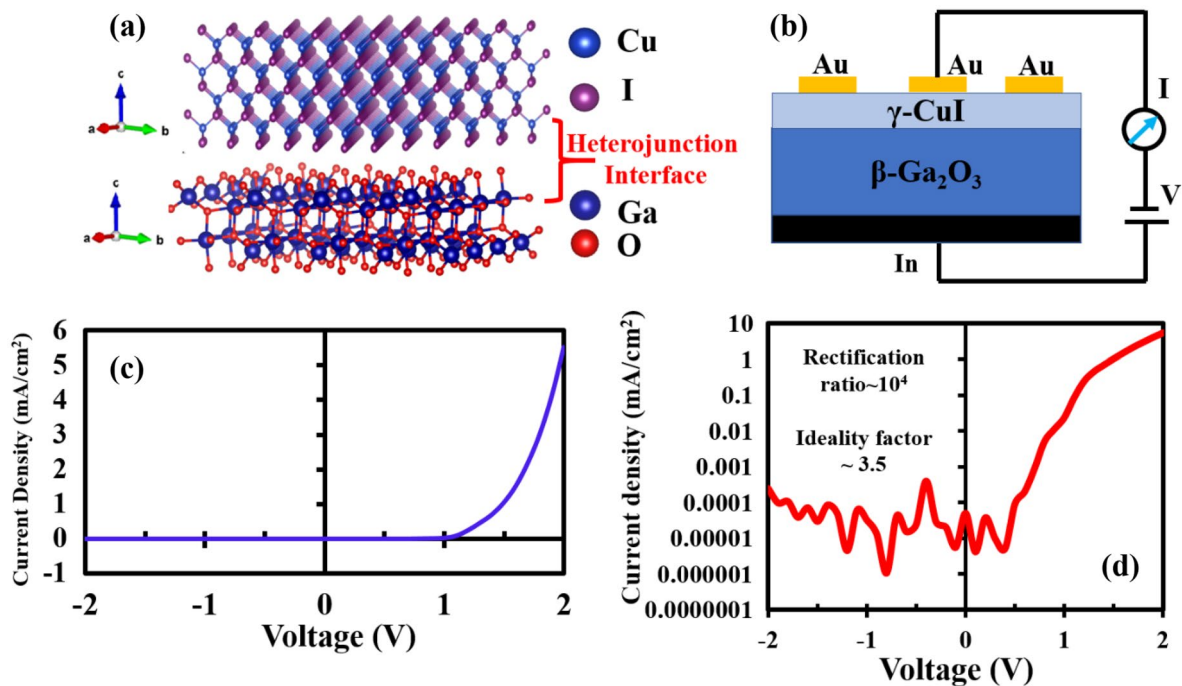


Fig. 2 **a** cross-section stick and ball crystal structure of  $\gamma$ -CuI and  $\beta$ -Ga<sub>2</sub>O<sub>3</sub>; **b** schematic of the fabricated vertical heterojunction device of  $\gamma$ -CuI and  $\beta$ -Ga<sub>2</sub>O<sub>3</sub>; **c** J–V characteristics; and **d** log plot of the J–V curve of the fabricated device for a voltage range of –2 V to 2 V

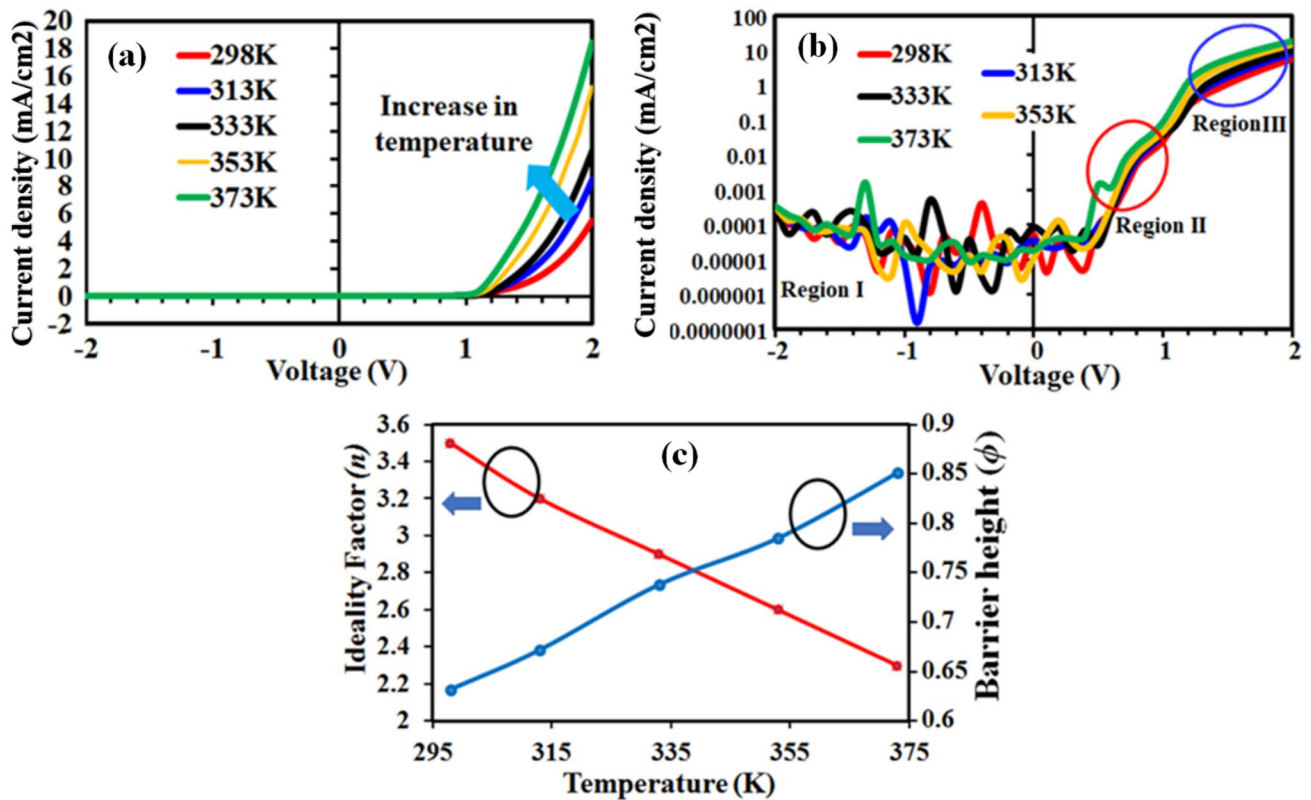
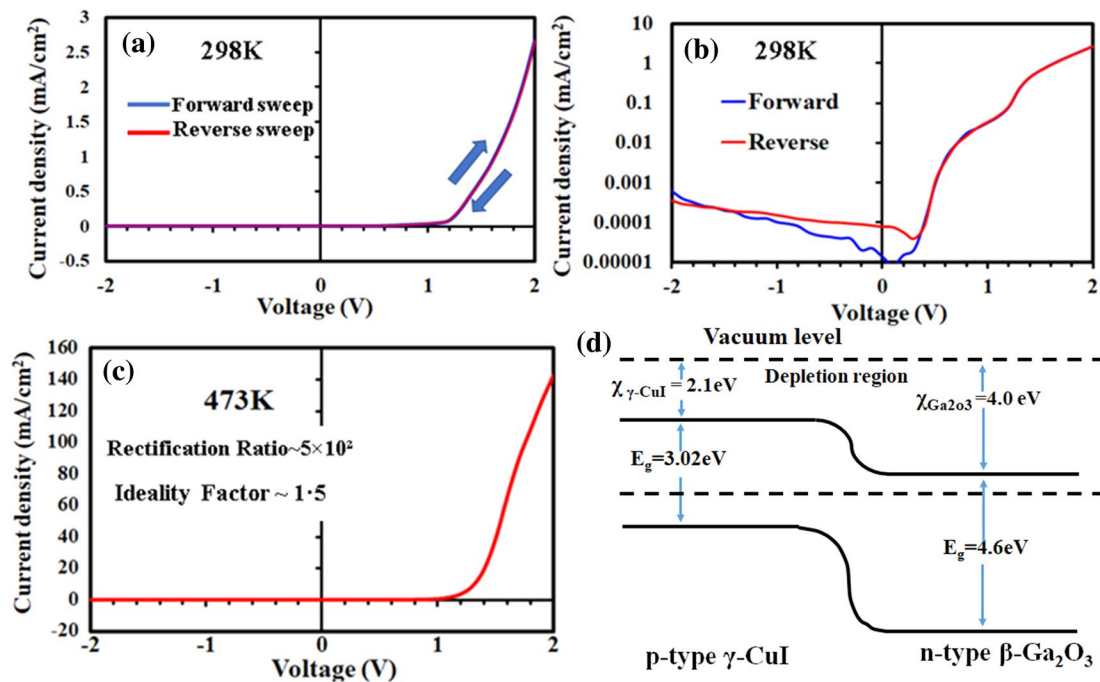


Fig. 3 **a** J–V characteristics in the temperature range 298–373 K and voltage range of –2 to 2 V; **b** Logarithm plot in the voltage range of –2 to 2 V, representing the current transport behavior for

the Au/ $\gamma$ -CuI/ $\beta$ -Ga<sub>2</sub>O<sub>3</sub>/In heterojunction device for the temperature range 298–373 K; **c** Variation in the ideality factor ( $n$ ) and barrier height ( $\phi$ ) with an applied temperature in the range 298–373 K



**Fig. 4** **a** J–V characteristics for the forward and reverse sweep of bias voltage; **b** Log plot of the J–V curve at room temperature (298 K); **c** J–V characteristics of the Au/ $\gamma$ -CuI/ $\beta$ -Ga<sub>2</sub>O<sub>3</sub>/In hetero-

junction device at a significantly higher temperature of 473 K with excellent rectification characteristics; and **d** energy bandgap diagram of the  $\gamma$ -CuI/ $\beta$ -Ga<sub>2</sub>O<sub>3</sub> heterojunction device in equilibrium

the experimental results suggest that the observed barrier inhomogeneity from the temperature-dependent J–V analysis can be correlated with the electrical hysteresis of the diode characteristics, which signifies the presence of surface defects and interface states.

## 4 Conclusions

We investigated the temperature-dependent device characteristics of the p-type  $\gamma$ -CuI and n-type  $\beta$ -Ga<sub>2</sub>O<sub>3</sub> heterojunctions, thereby analyzing the interface properties. A predominantly (111)-oriented cubic-phase  $\gamma$ -CuI was deposited on a  $\beta$ -Ga<sub>2</sub>O<sub>3</sub> substrate by evaporation. The fabricated  $\gamma$ -CuI/ $\beta$ -Ga<sub>2</sub>O<sub>3</sub> heterojunction showed excellent diode characteristics with a high rectification ratio and low reverse saturation current at 298 K, in the presence of a large barrier height of 0.632 eV. A decrease in the ideality factor and an increase in barrier height were observed when the temperature was increased from 298 to 373 K, indicating a barrier inhomogeneity at the heterojunction interface due to the surface defects present there. The electrical analysis also showed a small hysteresis effect on the reverse saturation current for the fabricated  $\gamma$ -CuI/ $\beta$ -Ga<sub>2</sub>O<sub>3</sub> heterojunction. The presence of electrical hysteresis for the reverse saturation current and the barrier inhomogeneity in the temperature-dependent

characteristics indicates the presence of some level of interface states. Irrespective of the existence of surface defects and interface states, a rectifying diode characteristic was obtained at temperatures as high as 473 K for the fabricated  $\gamma$ -CuI/ $\beta$ -Ga<sub>2</sub>O<sub>3</sub> heterojunction. Our study revealed that the electrical hysteresis and temperature-dependent electrical characteristics of the  $\beta$ -Ga<sub>2</sub>O<sub>3</sub>-based heterojunction device could be significant and correlated in identifying interface properties.

**Acknowledgements** We would like to thank Editage ([www.editage.com](http://www.editage.com)) for English language editing.

## Declarations

**Conflict of interest** The authors declare that there is no possible conflict of interest.

**Consent for publication** All authors has given the consent for publication of research.

**Open Access** This article is licensed under a Creative Commons Attribution 4.0 International License, which permits use, sharing, adaptation, distribution and reproduction in any medium or format, as long as you give appropriate credit to the original author(s) and the source, provide a link to the Creative Commons licence, and indicate if changes were made. The images or other third party material in this article are included in the article's Creative Commons licence, unless indicated otherwise in a credit line to the material. If material is not

included in the article's Creative Commons licence and your intended use is not permitted by statutory regulation or exceeds the permitted use, you will need to obtain permission directly from the copyright holder. To view a copy of this licence, visit <http://creativecommons.org/licenses/by/4.0/>.

## References

- Baldini M, Galazka Z, Wagner G (2018) Recent progress in the growth of  $\beta$ -Ga<sub>2</sub>O<sub>3</sub> for power electronics applications. *Mater Sci Semicond Process* 78:132–146
- Chabak KD, McCandless JP, Moser NA, Green AJ, Mahalingam K, Crespo A, Hendricks N, Howe BM, Tetlak SE, Leedy K, Fitch RC, Wakimoto D, Sasaki K, Kuramata A, Jessen GH (2018) Recessed-gate enhancement-mode  $\beta$ -Ga<sub>2</sub>O<sub>3</sub> MOSFETs. *IEEE Electron Dev Lett* 39:67–70
- Oishi T, Koga Y, Harada K, Kasu M (2015) High-mobility  $\beta$ -Ga<sub>2</sub>O<sub>3</sub>(201) single crystals grown by edge-defined film-fed growth method and their Schottky barrier diodes with Ni contact. *Appl Phys Express* 8:031101
- Ma N, Tanen N, Verma A, Guo Z, Luo T, Xing HG, Jena D (2016) Intrinsic electron mobility limits in  $\beta$ -Ga<sub>2</sub>O<sub>3</sub>. *Appl Phys Lett* 109:212101
- Kim M, Seo JH, Singiseti U, Ma Z (2017) Recent advances in free-standing single crystalline wide band-gap semiconductors and their applications: GaN, SiC, ZnO,  $\beta$ -Ga<sub>2</sub>O<sub>3</sub>, and diamond. *Mater Chem C* 5:8338
- Xu J, Zheng W, Hiang F (2019) Gallium oxide solar-blind ultraviolet photodetectors: a review. *J Mater Chem C* 7:8753–8770
- Pratiyush AS, Krishnamoorthy S, Muralidharan R, Rajan S, Nath DN (2019) 16: Advances in Ga<sub>2</sub>O<sub>3</sub> solar-blind UV photodetectors, gallium oxide technology, devices and applications, metal oxide. OSA Publications China, pp 365–399
- Higashiwaki M, Murakami H, Kumagai Y, Kuramata A (2016) Current status of Ga<sub>2</sub>O<sub>3</sub> power devices. *J Appl Phys* 55:1202
- Oshima T, Okuno T, Arai N, Suzuki N, Ohira S, Fujita S (2008) Vertical solar-blind deep-ultraviolet Schottky photodetectors based on  $\beta$ -Ga<sub>2</sub>O<sub>3</sub> substrates. *Appl Phys Express* 1:011202
- Jia M, Wang F, Tang L, Xiang J, Teng KS, Lau SP (2020) High-performance deep ultraviolet photodetector based on NiO/ $\beta$ -Ga<sub>2</sub>O<sub>3</sub> heterojunction. *Nanoscale Res Lett* 15:47
- Kim H, Tarelkin S, Polyakov A, Troschiev S, Nosukhin S, Kuznetsov M, Kim J (2020) Ultrawide-bandgap p-n heterojunction of diamond/ $\beta$ -Ga<sub>2</sub>O<sub>3</sub> for a solar-blind photodiode. *ECS J Solid State Sci Technol* 9:045004
- Farzana E, Zhang Z, Paul PK, Arehart AR, Ringel SA (2017) Influence of metal choice on (010)  $\beta$ -Ga<sub>2</sub>O<sub>3</sub> Schottky diode properties. *Appl Phys Lett* 110:202102
- Konishi K, Goto K, Murakami H, Kumagai Y, Kuramata A, Yamakoshi S, Higashiwaki M (2017) 1-kV vertical Ga<sub>2</sub>O<sub>3</sub> field-plated Schottky barrier diodes. *Appl Phys Lett* 110:103506
- Lin R, Zheng W, Zhang D, Zhang Z, Liao Q, Yang L, Huang F (2018) High-performance graphene/ $\beta$ -Ga<sub>2</sub>O<sub>3</sub> heterojunction deep-ultraviolet photodetector with hot-electron excited carrier multiplication. *ACS Appl Mater Interfaces* 26:22419
- Zhang J, Han S, Cui M, Xu X, Li WL, Xu H, Jin C, Gu M, Chen L, Zhang KHL (2020) Fabrication and interfacial electronic structure of wide bandgap NiO and Ga<sub>2</sub>O<sub>3</sub> p-n heterojunction. *ACS Appl Electron Mater* 2:456–463
- Zhuo R, Wu D, Wang Y, Wu E, Jia C, Shi Z, Xu T, Tiana Y, Li X (2018) A self-powered solar-blind photodetector based on a MoS<sub>2</sub>/ $\beta$ -Ga<sub>2</sub>O<sub>3</sub> heterojunction. *J Mater Chem C* 6:10982–10986
- Yamada N, Ino R, Tomura H, Kondo Y, Ninomiya Y (2017) High-mobility transparent p-type CuI semiconducting layers fabricated on flexible plastic sheets: toward flexible transparent electronics. *Adv Electron Mater* 3(12):1700298
- Ranade AK, Pradeep D, Mahyavanshi R, Tanemura M, Kalita G (2019) Formation of effective CuI-GaN heterojunction with excellent ultraviolet photoresponsive photovoltage. *Phys Status Solidi A* 216:1900200
- Yang C, Knei M, Schein FL, Lorenz M, Grundmann M (2016) Room-temperature domain epitaxy of copper iodide thin films for transparent CuI/ZnO heterojunctions with high rectification ratios larger than 109. *Sci Rep* 6:21937
- Ayhan ME, Shinde M, Todankar B, Pradeep D, Ranade AK, Tanemura M, Kalita G (2020) Ultraviolet radiation-induced photovoltaic action in  $\gamma$ -CuI/ $\beta$ -Ga<sub>2</sub>O<sub>3</sub> heterojunction. *Mater Lett* 262:127074
- Li S, Zhi Y, Lu C, Wu C, Yan Z, Liu Z, Yang J, Chu X, Guo D, Li P, Wu Z, Tang W (2020) Broadband ultraviolet self-powered photodetector constructed on exfoliated  $\beta$ -Ga<sub>2</sub>O<sub>3</sub>/CuI core-shell microwire heterojunction with superior reliability. *J Phys Chem Lett* 12:447–453
- Gallagher JC, Koehler AD, Tadjer MJ, Mahadik NA, Anderson TJ, Budhathoki S, Law KM, Hauser AJ, Hobart KD, Kub FJ (2019) Demonstration of CuI as a p-n heterojunction to  $\beta$ -Ga<sub>2</sub>O<sub>3</sub>. *Appl Phys Express* 12:104005
- Ranade AK, Mahyavanshi RD, Desai P, Kato M, Tanemura M, Kalita G (2019) Ultraviolet light induced electrical hysteresis effect in graphene-GaN heterojunction. *Appl Phys Lett* 114:151102
- Fares C, Ren F, Hays DC, Gila BP, Tadjer M, Hobart KD, Pearson SJ (2018) Valence band offsets for CuI on (-201) bulk Ga<sub>2</sub>O<sub>3</sub> and epitaxial (010) Al<sub>0.14</sub>Ga<sub>0.86</sub>O<sub>3</sub>. *Appl Phys Lett* 113:182101
- Yamada N, Kondo Y, Ino R (2019) Low-temperature fabrication and performance of polycrystalline CuI films as transparent p-type semiconductors. *Phys Status Solidi* 216:1700782
- Yang C, Souchay D, Kneiß M, Bogner M, Wei HM, Lorenz M, Oeckler O, Benstetter G, Fu YQ, Grundmann M (2017) Transparent flexible thermoelectric material based on non-toxic earth-abundant p-type copper iodide thin film. *Nat Commun* 8:1–7
- Kalita G, Mahyavanshi RD, Desai P, Ranade AK, Kondo M, Dewa T, Tanemura M (2018) Photovoltaic action in graphene-Ga<sub>2</sub>O<sub>3</sub> heterojunction with deep-ultraviolet irradiation. *Phys Status Solidi RRL* 12:1800198
- López I, Nogales E, Hidalgo P, Méndez B, Piqueras J (2012) Field emission properties of gallium oxide micro- and nanostructures in the scanning electron microscope. *Phys Status Solidi* 209:113–117
- Michaelson HB (1977) The work function of the elements and its periodicity. *J Appl Phys* 48:4729–4733
- Kalita G, Shaarin MD, Paudel B, Mahyavanshi R, Tanemura M (2017) Temperature dependent diode and photovoltaic characteristics of graphene-GaN heterojunction. *Appl Phys Lett* 111:013504
- Fares C, Ren F, Hays DC, Gila BP, Tadjer M, Hobart KD, Pearson SJ (2018) Valence band offsets for CuI on (-201) bulk Ga<sub>2</sub>O<sub>3</sub> and epitaxial (010) Al<sub>0.14</sub>Ga<sub>0.86</sub>O<sub>3</sub>. *Appl Phys Lett* 113:182101
- Zhang ZW, Lin RC, Li TT, Zhang ZJ, Huang F (2018) High quality  $\beta$ -Ga<sub>2</sub>O<sub>3</sub> film grown with N<sub>2</sub>O for high sensitivity solar-blind ultraviolet photodetector with fast response speed. *J Alloys Compd* 735:150–154
- Alonso M, Cimino R, Horn K (1990) Surface photovoltage effects in photoemission from metal-GaP(110) interfaces: importance for band bending evaluation. *Phys Rev Lett* 64:1947–1950
- Woodall JM, Islam MS, Kaya A, Dryden DM, Mao H, Alhalaili B (2017) Oxidation of GaAs substrates to enable  $\beta$ -Ga<sub>2</sub>O<sub>3</sub> films for sensors and optoelectronic devices. In: *Matin M, Dutta AK, Chowdhury S (eds) Wide bandgap power devices and application II*. SPIE, p 11



35. Mohamed M, Irmscher K, Janowitz C, Galazka Z, Manzke R, Fornari R (2012) Schottky barrier height of Au on the transparent semiconducting oxide  $\beta$ -Ga<sub>2</sub>O<sub>3</sub>. *Appl Phys Lett* 101:132106
36. Schein FL, Von Wenckstern H, Grundmann M (2013) Transparent p-CuI/n-ZnO heterojunction diodes. *Appl Phys Lett* 102:92109
37. Motaung DE, Mhlongo GH, Makgwane PR, Dhonge BP, Cummings FR, Swart HC, Ray SS (2018) Ultra-high sensitive and selective H<sub>2</sub> gas sensor manifested by interface of n-n heterostructure of CeO<sub>2</sub>-SnO<sub>2</sub>. *Sens Actuator B Chem* 254:984–995

**Publisher's Note** Springer Nature remains neutral with regard to jurisdictional claims in published maps and institutional affiliations.